SHEARLET FEATURES FOR REGISTRATION OF REMOTELY SENSED MULTITEMPORAL IMAGES

James M. Murphy [1,2]*, Jacqueline Le Moigne* [2]
[1]University of Maryland, College Park
[2]NASA Goddard Space Flight Center

ABSTRACT

We investigate the role of anisotropic feature extraction methods for automatic image registration of remotely sensed multitemporal images. Building on the classical use of wavelets in image registration, we develop an algorithm based on shearlets, a mathematical generalization of wavelets that offers increased directional sensitivity. Initial experimental results on LANDSAT images are presented, which indicate superior performance of the shearlet algorithm when compared to classical wavelet algorithms.

***Index Terms*—** Image registration, shearlets, wavelets, optimization, remotely-sensed, multitemporal, LANDSAT.

1 Introduction

The problem of accurately and robustly registering multitemporal image data is a significant problem in the field of remote sensing. Images of the same scene, captured by the same sensor, can have severe misalignment if taken at different times. This can be due to seasonal changes, cloud coverage, and differences in sensor placement. In order to register two such scenes, techniques developed from the mathematical discipline of harmonic analysis have been successful.

In particular, methods based on *wavelets* have been effectively applied to the problem of registering multitemporal, remotely-sensed images [1]. By decomposing an image according to a discrete wavelet algorithm, an image is reduced to more essential features, which are easier to match. It is well-known that wavelets capture certain features of an image, such as textures, quite well. Their simple and fast implementation through a variety of filter schemes has also contributed to the success of wavelets and related algorithms, such as Simoncelli steerable filters [2].

However, wavelets are known to be *isotropic*, meaning they do not effectively represent images that have directional features. This theoretical limitation to wavelets has been known since the beginning of their study [3], and puts limitations on their effectiveness in analyzing certain image classes. In particular, images with strong edge-like features, including rivers, roads, and mountains, are not optimally represented with wavelet-like algorithms.

Anisotropic generalizations of wavelets abound. In particular, *shearlets* [4], [5] give a fast, optimized, and directionally-dependent decomposition of images, which we shall show yield a robust algorithm for the registration of multitemporal images.

2 Background on Wavelets and Shearlets

In a broad sense, wavelet algorithms decompose an image with respect to *scale* and *translation*. Mathematically, for a signal $f \in L^2([0,1]^2)$, understood as an ideal image signal, and an appropriately chosen wavelet function ψ, f may be decomposed as

$$f \sim \sum_{m=-\infty}^{\infty} \sum_{n \in \mathbb{Z}^2} \langle f, \psi_{m,n} \rangle \psi_{m,n}, \tag{1}$$

where $\psi_{m,n}(x) = 2^{\frac{m}{2}}\psi(A^m x - n)$ and $A = \begin{pmatrix} 2 & 0 \\ 0 & 2^{\frac{1}{2}} \end{pmatrix}$. The collection of wavelet coefficients $\{\langle f, \psi_{m,n}\rangle\}_{m\in\mathbb{Z},n\in\mathbb{Z}^2}$ describes the behavior of f, our image signal, at different scales (determined by m) and at different translations (determined by n). This continuous scheme is discretized to work with real, discrete image signals.

Shearlets generalize wavelets by decomposing with respect not just to *scale* and *translation*, but also *direction*. Mathematically, given a signal $f \in L^2(\mathbb{R}^2)$ and an appropriate base function ψ, we may decompose f as

$$f \sim \sum_{i=-\infty}^{\infty} \sum_{j=-\infty}^{\infty} \sum_{k\in\mathbb{Z}^2} \langle f, \psi_{i,j,k}\rangle \psi_{i,j,k}, \qquad (2)$$

where:

- $\psi_{i,j,k}(x) = 2^{\frac{3i}{4}}\psi(B^j A^i x - k)$.
- $A = \begin{pmatrix} 2 & 0 \\ 0 & 2^{\frac{1}{2}} \end{pmatrix}$, $B = \begin{pmatrix} 1 & 1 \\ 0 & 1 \end{pmatrix}$.

The new matrix B is a shearing matrix, and adds a directional component to our decomposition. The shearlet coefficients $\{\langle f, \psi_{i,j,k}\rangle\}_{i,j\in\mathbb{Z},k\in\mathbb{Z}^2}$ describe the behavior of f at different scales (determined by i), translations (determined by k) and directions (determined by j).

The role of shearlets in automatic image registration can be understood heuristically as follows: shearlets produce sparse, concentrated, and directional features in images, which give the optimization algorithm used for image registration sparse, concentrated features with which to match.

We hypothesized these sparse, concentrated features would allow us to register multitemporal images that begin severely misaligned. More precisely, we hypothesized the sparsity of our shearlet features would produce a more robust registration algorithm, compared to one based on classical wavelets. Initial results confirming this heuristic argument are discussed in section 4.

3 REGISTRATION ALGORITHM DESIGN

Our image registration algorithm is based on decomposing the input and reference images using harmonic analysis tools. Our ambition is to compare isotropic wavelet-like methods to an anisotropic generalization, shearlets. To do so, we consider wavelet-like algorithms in the form of spline wavelets and Simoncelli steerable pyramids [6], and the fast shearlet transform [7]. These features are then matched using a non-linear least squares optimization algorithm, in order to compute the registration transformation between the images.

We summarize our image registration algorithm in terms of the four components of image registration described by Brown [8]:

1. *Search Space:* Rotation and translation.
2. *Features*: Wavelet features in one case and shearlet features in another.
3. *Similarity Metric*: Unconstrained least squares. That is, if F_R and F_I are the reference and input features, N the number of relevant pixels, (x_i, y_i) the integer coordinate of the ith pixel, and T_p the transformation associated to parameters p, we seek to minimize the similarity metric given by:

$$\chi^2(p) = \frac{1}{N}\sum_{i=1}^{N} \left(F_R(T_p(x_i, y_i)) - F_I(x_i, y_i)\right)^2.$$

4. *Search Strategy:* Modified Marquadt-Levenberg method of solving non-linear least squares problems [9], [10].

4 INITIAL EXPERIMENTAL RESULTS

To test our wavelet and shearlet algorithms, we registered multitemporal images produced by Landsat-5 TM and Landsat-7 ETM+ sensors. These images have been processed by USGS EROS Data Center, by removing artifacts and resampling. The images may be seen in

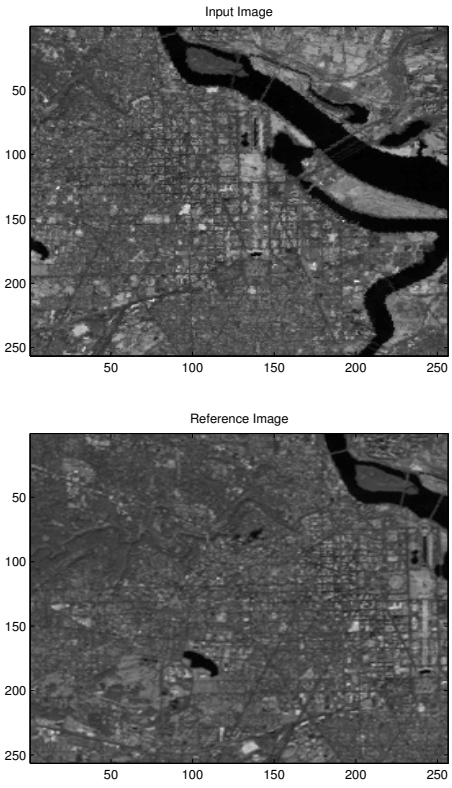

Fig. 1. Input and Reference Multitemporal Images.

Figure 1. Notice the large displacement between the two images. Indeed, using ENVI software tools, manual registration was performed on the images to compute an RST transformation between them. The manual registration parameters are: $(T_x, T_y, \theta) = (103.2, -8.1, 0)$. This is an exceptionally large translation in the y direction, so this image pair constitutes a severe misalignment.

We performed automatic image registration with wavelet-like features and shearlet features, and compared the results to this manual registration. We allowed the initial guess of the registration, denoted $(T_{x_0}, T_{y_0}, \theta_0)$, to increase towards the true registration, to determine the robustness of the algorithms. The further the initial guess from the true registration, the more robust a registration algorithm is if it converges to the correct registration. The results of our registration experiments may be seen in Tables 1, 2, 3, 4.

$(T_{x_0}, T_{y_0}, \theta_0)$	Spline Wavelets	Shearlets
(0,0,0)	(-1.5, 1.1, -2.4)	(-.1, .3, .1)
(10, -1, 0)	(10.2, -.6, .1)	(62.6, 33.1, 8.54)
(20, -2, 0)	(18.4, -1.8, -1.0)	(64.8, 30.3, .1)
(30, -3, 0)	(29.6, -2.7, -.2)	**(103.6, -8.2, .1)**
(40, -4, 0)	(39.3, -4.5, -1.3)	**(103.6, -8.2, .1)**
(50, -5, 0)	(39.3, 4.0, -1.3)	**(103.6, -8.2, .1)**
(60, -6, 0)	(62.9, -1.0, -.1)	**(103.6, -8.2, .1)**
(70, -7, 0)	(70.9, -.2, -1.2)	**(103.6, -8.2, .1)**
(80, -8, 0)	**(103.5, -8.0, 0)**	**(103.6, -8.2, .1)**
(90, -9, 0)	**(103.5, -8.0, 0)**	**(103.6, -8.2, .1)**
(100, -10, 0)	**(103.5, -8.0, 0)**	**(103.6, -8.2, .1)**

Table 1. Comparison of spline wavelets to shearlets. Bold entries indicate convergent registrations. The spline wavelets algorithm begins to converge at $(80, -8, 0)$, the shearlets algorithm at $(30, -3, 0)$.

Tables 1 and 2 indicate superior robustness of shearlets when compared to spline wavelets or Simoncelli band-pass features. Table 3 is ambiguous as to which of shearlets or Simoncelli low-pass is more robust for these multitemporal images, but more subtle choices of initial guesses in Table 4 indicate the superior robustness of shearlets in this case as well.

More comprehensive statistical analysis of these image registration experiments, as well as experiments with other multitemporal images are in progress, and shall be presented at the conference.

5 References

[1] Nathan S. Netanyahu, Jacqueline Le Moigne, and Jeffrey G. Masek, "Georegistration of landsat data via robust matching of multiresolution features," *IEEE Transactions on Geoscience and Remote Sensing*, vol. 42, no. 7, pp. 1586–1600, 2004.

[2] E. Simoncelli, W. Freeman, E. Adelson, and D. Heeger, "Shiftable multiscale transforms," *IEEE Transactions on Information Theory*, vol. 38, no. 3, pp. 587–607, 1992.

[3] Ingrid Daubechies, *Ten lectures on wavelets*, Society for industrial and applied mathematics, 1992.

$(T_{x_0}, T_{y_0}, \theta_0)$	Sim.-Band	Shearlets
(0,0,0)	(.5, 3.4 -6.6)	(-.1, .3, .1)
(10,-1, 0)	(10.8, 14.9, -4.5)	(62.6, 33.1, 8.54)
(20, -2, 0)	(10.8, 14.8, -4.6)	(64.8, 30.3, .1)
(30, -3, 0)	(30.1, -3.0, 0)	**(103.6, -8.2, .1)**
(40, -4, 0)	(42.3, -1.8, -13.3)	**(103.6, -8.2, .1)**
(50, -5, 0)	(48.1, 4.9, -3.8)	**(103.6, -8.2, .1)**
(60, -6, 0)	(61.3, -1.2, .6)	**(103.6, -8.2, .1)**
(70, -7, 0)	(60.8, 12.8, .8)	**(103.6, -8.2, .1)**
(80, -8, 0)	**(103.5, -8.0, .1)**	**(103.6, -8.2, .1)**
(90, -9, 0)	**(103.5, -8.0, .1)**	**(103.6, -8.2, .1)**
(100, -10, 0)	**(103.5, -8.0, .1)**	**(103.6, -8.2, .1)**

Table 2. Comparison of Simoncelli band-pass features to shearlets. Bold entries indicate convergent registrations. The Simoncelli band-pass algorithm begins to converge at $(80,-8,0)$, the shearlets algorithm at $(30,-3,0)$.

$(T_{x_0}, T_{y_0}, \theta_0)$	Sim.-Low	Shearlets
(0,0,0)	(-12.2, 2.2, -14.7)	(-.1, .3, .1)
(10, -1, 0)	(19.2, 6.8, -10.0)	(62.6, 33.1, 8.54)
(20, -2, 0)	(41.9, -.9, -12.3)	(64.8, 30.3, .1)
(30, -3, 0)	**(103.5, -8.0, .1)**	**(103.6, -8.2, .1)**
(40, -4, 0)	**(103.5, -8.0, .1)**	**(103.6, -8.2, .1)**
(50, -5, 0)	**(103.5, -8.0, .1)**	**(103.6, -8.2, .1)**
(60, -6, 0)	**(103.5, -8.0, .1)**	**(103.6, -8.2, .1)**
(70, -7, 0)	**(103.5, -8.0, .1)**	**(103.6, -8.2, .1)**
(80, -8, 0)	**(103.5, -8.0, .1)**	**(103.6, -8.2, .1)**
(90, -9, 0)	**(103.5, -8.0, .1)**	**(103.6, -8.2, .1)**
(100, -10, 0)	**(103.5, -8.0, .1)**	**(103.6, -8.2, .1)**

Table 3. Comparison of Simoncelli low-pass features to shearlets, first analysis. Bold entries indicate convergent registrations. Both the Simoncelli low-pass algorithm and the shearlets algorithm begin to converge at $(30,-3,0)$.

$(T_{x_0}, T_{y_0}, \theta_0)$	Sim.-Low	Shearlets
(5, -8, ,0)	(-8.0, -10.9, -12.2)	**(103.6, -8.1, 0)**
(10, -8, 0)	(-13.5, 2.1, -14.6)	**(103.6, -8.2, 0)**
(20, -8, 0)	(14.5, -8.3, -2.6)	**(103.6, -8.2, 0)**

Table 4. Comparison of Simoncelli low-pass features to shearlets, second analysis. Bold entries indicate convergent registrations. When the T_{y_0} parameter is fixed near the correct value, shearlets have superior robustness near the critical threshold of $T_{x_0} = 30$.

[4] Kanghui Guo and Demetrio Labate, "Optimally sparse multidimensional representation using shearlets," *SIAM journal on mathematical analysis*, vol. 39, no. 1, pp. 298–318, 2007.

[5] Glenn R. Easley, Demetrio Labate, and Wang-Q. Lim, "Sparse directional image representations using the discrete shearlet transform," *Applied and Computational Harmonic Analysis*, vol. 25, no. 1, pp. 25–46, 2008.

[6] Ilya Zavorin and Jacqueline Le Moigne, "Use of multiresolution wavelet feature pyramids for automatic registration of multisensor imagery," *IEEE Transactions on Image Processing*, vol. 14, no. 6, pp. 770–782, 2005.

[7] Sören Häuser, "Fast finite shearlet transform," *arXiv preprint*, vol. arXiv:1202.1773, 2012.

[8] Lisa Gottesfeld Brown, "A survey of image registration techniques," *ACM computing surveys*, vol. 24, no. 4, pp. 325–376, 1992.

[9] D.W. Marquadt, "An algorithm for least-squares estimation of non-linear parameters," *Journal of SIAM*, vol. 11, pp. 431–441, 1963.

[10] Philippe Thévenaz, Urs E. Ruttiman, and Michael Unser, "A pyramid approach to subpixel registration based on intensity," *IEEE Transactions on Image Processing*, vol. 7, no. 1, pp. 27–41, 1998.